Spatial Resolution Characteristics of K-L Domain Adaptive Wiener Filtering on SPECT Sinogram Poisson Noise

Hongbing Lu and Zhengrong Liang

***Abstract*—This work investigated a Karhunen-Loeve (K-L) domain adaptive Wiener filtering of correlated sinogram data, in terms of noise reduction and resolution preservation. By adding Anscombe transform, this approach provides a means for accurate treatment of Poisson noise for SPECT (single photon emission computed tomography). The Anscombe transform stabilizes the signal-dependent Poisson process with a nearly constant variance. The K-L transform manipulates the stabilized sinogram into ordered principal components with their correspondingly ordered signal-to-noise ratios (SNRs). Given the SNRs, a Wiener filter can be accurately designed for an adaptive penalized minimum least-square noise smoothing on each principal component. A three-dimensional (3D) spatial noise filtering across the field-of-view then becomes a series of 2D process adaptive to each principal component, which can be implemented efficiently by parallelization. Performance of this adaptive Poisson noise treatment was evaluated by simulated SPECT studies in terms of local impulse response and noise-resolution tradeoff with comparison to the conventional low-pass noise filters. The evaluation indicates the potential of the presented method for analytical inversion of the attenuated Radon transform in the presence of Poisson noise.**

***Index Terms*—Sinogram Poisson noise reduction, adaptive Wiener filtering, K-L transform, Anscombe transform, local impulse response, resolution uniformity.**

I. Introduction

INversion of the attenuated Radon transform for quantitative SPECT (single photon emission computed tomography) has become feasible [1, 2] due to the work of Novikov [3, 4], even for 180° data sampling [5-8]. Extension to include collimation and scatter effects has also become feasible [7, 9]. A major obstacle for the inversion-based approach to practical use is the signal-dependent Poisson noise [10]. Current practice utilizes a spatially-invariant low-pass filter, such as Hanning, to smooth the non-stationary noise frame-by-frame or projection-by-projection. Extension to consider the signal-dependent nature has been explored [11, 12]. Further investigation by filtering all the projection images together (i.e., filtering the sinogram which contains the angular correlation among the projections) has also been explored with improvement over filtering images individually [13, 14]. It has been recognized that Karhunen-Loeve (K-L) transform has a unique advantage in handling correlative signals [15-17]. Incorporating this transform for accurate treatment of Poisson noise was investigated in [18], where the Anscombe transform [19] was employed to consider the non-stationary nature of the noise.

This work investigates the K-L domain Poisson noise treatment strategy in terms of local impulse response (LIR) and noise-resolution tradeoff (NRT) with comparison to the conventional low-pass filters and some previously reported results of other approaches.

II. Method and Materials

Noise-filtering problem in SPECT can be viewed as to estimate the means (or noise-free projections), given a single realization of jointly independent Poisson distributed projection data, where the means or signals have either temporal and/or spatial correlation due to the projection process. The estimation task here is to model accurately the signal-dependent noise nature within the K-L framework. There are several ways to handle the signal-dependence [20, 21], where the Anscombe transform is a simple and effective method which converts a Poisson process into a nearly Gaussian with a constant variance of 0.25. Since K-L transform is a linear operation, the noise modeling before and after the transform is equivalent. In this work, we perform the Anscombe transform prior to the K-L transform.

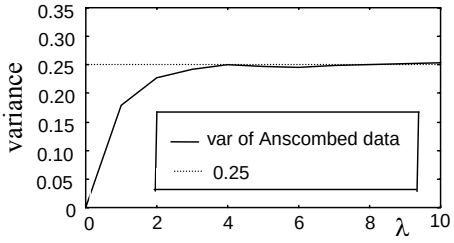

Figure 1: The variance in the Anscombe transformed data space.

A. Anscombe Transform

If x is Poisson distributed with mean equals to λ, then $y = (x+3/8)^{1/2}$ can be approximated as Gaussian distributed with mean equals to $(\lambda+1/8)^{1/2}$ and variance of 0.25. The variance starts to decrease toward zero when λ goes to zero from four.

B. K-L Transform

In the Anscombe space, y is nearly Gaussian with a constant variance for $\lambda > 4$, see Figure 1, (if a line integral is less than 4 at a detector bin, the measured noisy datum at that bin has no much information for those image voxels associated with the line integral). The linear K-L transform on sinogram $\mathbf{y}$, (i.e., $\mathbf{z} = A\mathbf{y}$, where A is the K-L transform matrix), will retain the properties of Gaussian distribution and constant variance [16, 17]. In other words, z is nearly Gaussian distributed with a constant variance of 0.25. In the

Manuscript received by January 17, 2005. The work of Lu was supported in part by the National Nature Science Foundation of China under Grant # 30170278 and the work of Liang was supported in part by the NIH Grant #HL51466.

Lu was with the Department of Radiology, State Univ of New York, Stony Brook, NY 11794, USA and now is with the Department of Biomedical Engineering, Fourth Military Medical University, Xi'an, Shaanxi, 710032, China. (phone +86-29-8337-4837; e-mail: luhb@fmmu.edu.cn). Liang is with the Departments of Radiology, Computer Science and Physics, State Univ of New York, Stony Brook, NY 11794, USA (phone: 631-444-7837; fax: 631-444-6450; e-mail: jzl@mil.sunysb.edu).

K-L domain, we obtain a series of ordered eigenvalues and correspondingly we have a series of ordered principal components. The eigenvalue is directly proportional to the signal variation of the corresponding principal component. Therefore, we have obtained the signal-to-noise ratio (SNR) for each principal component in the K-L domain. In addition to the signal information manipulation, the K-L transform also simplifies the numerical calculation. If the sinogram is a three-dimensional (3D) dataset (i.e., 2D detector-bin array plus the angular sampling), then each principal component is a 2D image. Operations on these images can be parallelized. Furthermore, those components may be discarded if their eigenvalues are very small [16, 17].

The K-L transform could be performed along three different directions, depending on the data sampling. In the image domain, the most nearby voxels have the strongest correlation, which is usually specified by a Markov random field model. This nearby voxel correlation is embedded in the line integrals or sinogram. A straightforward implementation of the K-L transform is among the nearby bins of each projection image [22]. Another implementation is along the nearby projections to consider the angular correlation [23]. For SPECT application with a significant collimation effect, the correlation along image slice or sinogram direction can be significant for the K-L transform [18]. In the following, we will focus on the third implementation. Comparison of these three different implementations will be reported below.

C. K-L Domain Adaptive Noise Filtering

Given the constant variance and Gaussian nature, a penalized minimum least-square estimation (PMLSE) can be established to treat the noise adaptively by the obtained SNR for each principal component. The minimization for each component can be numerically performed by a Wiener filter:

$$H_k(\omega_s,\omega_t)=\frac{S_{Z^k}(\omega_s,\omega_t)-\sigma_n{}^2}{S_{Z^k}(\omega_s,\omega_t)+(\beta-1)\sigma_n{}^2} \qquad (1)$$

where S_{Z^k} is the 2D power spectrum of the *k*-th principal component data $\mathbf{z}^k$ and (ω_s,ω_t) denote the 2D FT coordinates for spatial coordinates (*s*, *t*) of the *k*-th principal component. Notation β is a smoothing parameter, controlling the degree of smoothness. If it is equal to 1, a MLSE solution is obtained. If it is greater than 1, a PMLSE solution is approached. The Wiener filter of Eq.(1) contains explicitly the constant variance $\sigma_n^2 = 0.25$, while the signal is related to the power spectrum S_{Z^k}. An explicit relation between SNR and each principal component is given in [18].

III. Experimental Design and Results

Computer simulations were conducted to evaluate the performance of the presented K-L domain adaptive Wiener filtering of Poisson noise in the sinogram space, in terms of LIR and NRT on the reconstructed images using a standard filtered backprojection (FBP) method (i.e., with a unapodized Ramp filter at the Nyquist frequency cutoff). Since the standard FBP reconstruction does not alter the data noise properties, comparison to the conventional low-pass filters was performed using their FBP results. Comparison to previously reported results of other approaches was also reported.

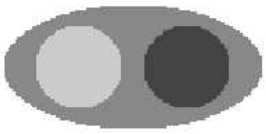

Figure 2: Digital phantom used to examine spatial resolution properties.

A. Experimental Design

To ensure a reliable comparison study, we first establish the baseline of FBP reconstruction and LIR measures. This baseline was measured by the resolution uniformity and isotropy. An elliptic digital phantom of 128 cubic size with a "hot" and "cold" disks was constructed, as shown in Figure 2. The two disk centers are at different locations off the phantom center. Three different count densities were simulated with relative emission intensities of 3, 2, and 1 in the hot disk (left), the background ellipse, and the cold disk (right), respectively, which allow us to test the dependence of LIR on different count levels. The phantom is essentially the same as that used in [24, 25]. Emission scans was simulated with 128 radial bins and 128 projection angles uniformly spaced over 360º by strip integrals. Attenuation, scatter and collimation effects were not considered for the purpose of this study, which focuses only on the projection mean estimation. Thus the simulated imaging system has intrinsically uniform and isotropic resolution. Any resolution effect would be due to the used filtering techniques. A total of 250 realizations of noisy projections were generated from the simulated noise-free projections using a Gaussian white noise generator (zero mean and variance equals to the average of the noise-free data). Emission images were reconstructed by the FBP method after the noisy projections were filtered by the Hanning filter, resulting in 250 images for an empirical LIR evaluation [24, 25]. From these 250 reconstructions, three LIRs each at the three pixels, which are located in the centers of the phantom and the two disks respectively, were computed. In addition, a linearized prediction of the LIR [24, 25] from noise-free FBP reconstruction was also computed. On the top of Figure 3 displays the horizontal profiles through the LIR functions from the FBP reconstructions. The circles denote the empirical results of LIR from the 250 noisy realizations with the Hanning filter (cutoff at 0.8 Nyquist frequency). The solid lines denote the linearized predictions of LIR from the standard FBP reconstruction of the noise-free projections. Agreement between the empirical results and the analytical prediction is clearly seen, especially in the neighborhood of the interested pixels. In addition to the resolution uniformity, the isotropic property at a given point in the reconstructed image is another important factor for consideration. On the bottom of Figure 3 displays the contours of the LIR functions at levels 25%, 50%, 75%, and 99% of the peak value for the three pixels of interest. As expected the spatially invariant low-pass Hanning filter provides isotropic FBP reconstruction for stationary noise, although some of other filters and reconstructed methods may lead to asymmetric LIRs [24, 25]. These results established the baseline of using FBP and LIR for measures of different

filters' performances.

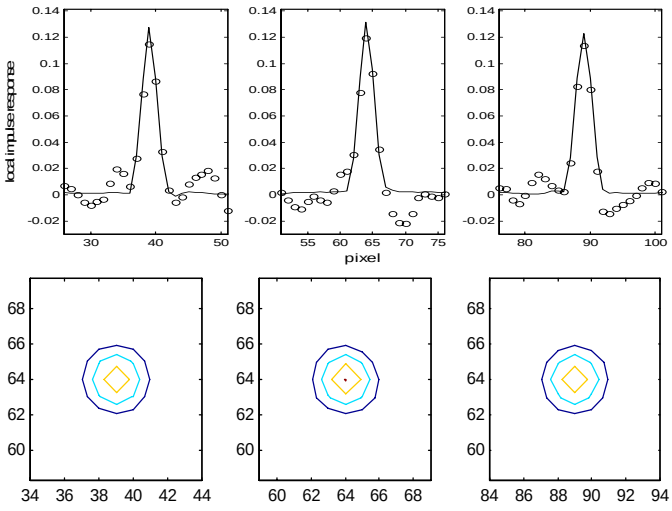

Figure 3: Top row shows the horizontal profiles, for the three pixels of interest respectively, through the three LIR functions of FBP reconstruction with Hanning filter (cutoff at 0.8 Nyquest frequency). The circles denote the empirical results from 250 noisy realizations and solid lines denote the linearized predictions of LIR. Bottom row shows the contours of the LIR functions at 25%, 50%, 75%, and 99% of the peak value for the three pixels of interest, respectively. From left to right: corresponding to the point at the center of the cold disk, the center of the image, and the center of the hot disk, respectively.

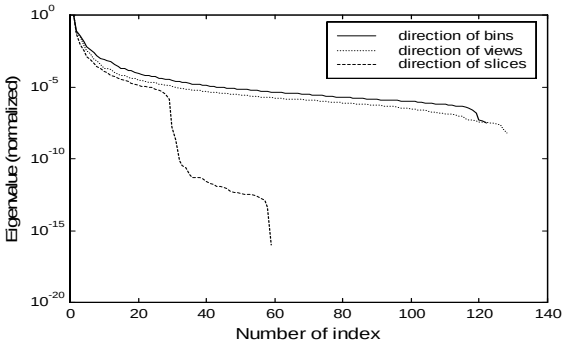

Figure 4: Spectra of the normalized eigenvalues of K-L transform along different directions. The horizontal axis shows the number of ordered principal components.

B. K-L Transform along Different Directions

The difference of K-L transform along the direction of bins, views, and slices, respectively, of a noise-free sinogram is shown by Figure 4, where the data was simulated from a 3D phantom modified from that of Figure 2 and the Anscombe transform was not applied. The disks in the 3D phantom become spheres. The signal distribution along the principal components is similar for K-L transform along the directions of bins and views. The transform along the direction of the slices or sinograms concentrates the signal distribution toward the first 60 among the 128 principal components. In other words, the K-L transform along the direction of the sinograms is more effective in concentrating the correlated signal distribution toward the major ordered principal components than that along the directions of the bins and views. Therefore, the K-L transform along the sinogram direction is chosen in the following studies.

C. LIR Measure on the K-L Domain Adaptive Filter

The data simulation for the results of Figure 3 was repeated using the modified 3D phantom. A total of 250 noisy realizations of Poisson nature from the noise-free projections were generated, Anscombe transformed, treated by the K-L domain adaptive Wiener filter and then reconstructed by the standard FBP method. Figure 5 shows the horizontal profiles through the three LIR functions (for the three pixels of interest) of the FBP reconstructions from the 250 noisy realizations. The LIRs at the centers of the hot and cold disks are at the same level, and the LIR at the center of the image is about 0.02 higher. This is a significant improvement as compared to other methods. For example, the percentage of the overshoot is more than 17% for the FBP reconstruction with Hanning filtering (cutoff at 0.8 Nyquest frequency) on the Poisson noise. This is expected since the spatially-invariant filter does not model the non-stationary nature of the Poisson noise. The uniformity performance of the K-L domain adaptive Wiener filtering on non-stationary noise is also superior as compared to iterative reconstructions, such as the penalized-likelihood estimation with a standard penalty (about 40% overshoot as estimated from [24]), and the penalized-likelihood estimation with a modified penalty (about 16% overshoot as estimated in [24]). It is recognized that it is a challenging task to achieve a uniform resolution in few iterations and to suppress the noise at higher iterations [26].

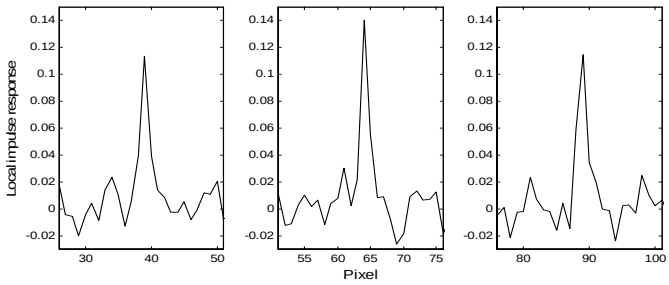

Figure 5: Horizontal profiles through the three LIR functions (for the three pixels of interest) from the FBP reconstructions with K-L domain adaptive Wiener filtering of the 250 noisy realizations. From left to right: at the center of the hot disk, the center of the image, and the center of the cold disk, respectively.

D. Noise-Resolution Tradeoff

It is well known that the cutoff frequency of Hanning filter (and other conventional filters) controls an overall tradeoff between noise and resolution: a lower cutoff frequency leads to coarser resolution but less noisy, and vice versa. For signal-dependent Poisson noise, a single cutoff frequency is not sufficient to achieve a good tradeoff for noise reduction and resolution preservation across the field-of-view. An adaptive process is desired. The analyses in sections above show that the proposed K-L domain Wiener filtering method can adaptively smooth the sinogram according to the SNRs of each principal component. This unique property of adaptive filtering the components independently and locally in the K-L domain is explored below in a more quantitative manner.

The NRT induced by the conventional methods and our approach were calculated, as shown in Figure 6. The resolution was measured by an average of full-width-at-half-maximum (FWHM) along the horizontal and vertical directions of each LIR, while the noise was measured by the empirical standard deviation. As discussed in the previous sections, the K-L domain adaptive Wiener filter is nonlinear,

so that the resolution properties for FBP with the proposed method were generated from the empirical estimation from the 250 realizations, while the resolution properties for FBP with the linear Hanning and Shepp-Logan filters were determined using the linearized predictions of LIR. The curves for the low-pass Hanning and Shepp-Logan filters reflect the NRT for different cutoff frequencies. The effects of the K-L domain adaptive Wiener filter were studied with the smoothing parameter β in Eq.(1) equals to 0.5, 1.0 , 2.0 and 5.0, respectively. In the figure, the NRT curves of the Hanning and Shepp-Logan filters follow an essentially similar trend, while all the data points from the presented adaptive filtering draw a curve much more close to the axes, indicating a superior tradeoff performance.

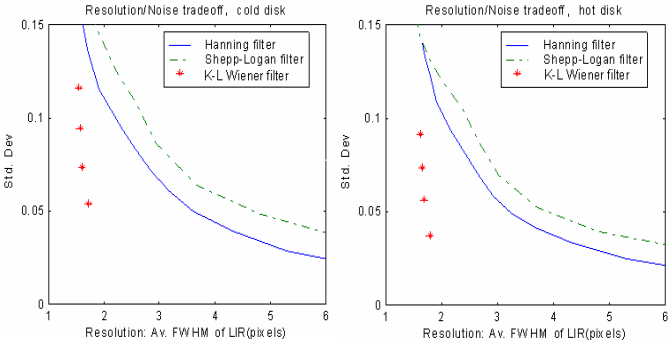

Figure 6: NRT at the centers of the cold disk and the hot disk for the FBP with K-L domain adaptive Wiener filter and Hanning/Shepp-Logan filters. Left is the result for the pixel at the center of the cold disk and right is the result for the pixel at the center of the hot disk.

IV. Discussion and Conclusion

The non-stationary noise in SPECT must be treated by corresponding methods, not the spatially-invariant low-pass linear filters. The presented K-L domain adaptive approach with the Anscombe transform is a choice so far to consider the non-stationary and correlative properties of the sinogram.

References

[1] L.A. Kunyansky, "A new SPECT reconstruction algorithm based on the Novikov explicit inversion formula", *Inverse Problems*, Vol. 17, pp. 293-306, 2001.

[2] F. Natterer, "Inversion of the attenuated Radon transform", *Inverse Problems*, Vol. 17, pp. 113-119, 2001.

[3] R.G. Novikov, "An inversion formula for the attenuated X-ray transformation", *Preprint*, May of 2000, and in *Ark. Math.*, Vol. 40, pp. 145-167, 2002.

[4] R.G. Novikov, "On the range characterization for the two-dimensional attenuated X-ray transformation", *Inverse Problems*, Vol. 18, pp. 677-700, 2002.

[5] H. Rullgård, "Stability of the inverse problem for the attenuated Radon transform with 180° data", *Inverse Problems*, Vol. 20, pp. 781-797, 2004.

[6] F. Noo and J.M. Wagner, "Image reconstruction in 2D SPECT with 180º acquisition", *Inverse Problems*, Vol. 17, pp. 1357-1371, 2001.

[7] X. Pan, E.Y. Sidky, C-M. Kao, Y. Zou, and C.E. Metz, "Short-scan SPECT imaging with non-uniform attenuation and 3D distance distance-dependent spatial resolution", *Phys. Med. Biol.*, Vol. 47, pp. 2811-33, 2002.

[8] X. Pan, C-M. Kao, E.Y. Sidky, Y. Zou, and C.E. Metz, "π -Scheme short-scan SPECT and image reconstruction with non-uniform attenuation", *IEEE Trans. Nucl. Science*, Vol. 50, pp. 87-96, 2003.

[9] H. Lu, J. Wen, X. Li, T. Li, G. Han, and Z. Liang, "Towards analytical solution for 3D SPECT reconstruction with non-uniform attenuation and distance-dependent resolution variation: A Monte Carlo simulation study", *SPIE Med. Imaging*, Vol. 4684, pp. 20-28, 2002.

[10] J-P Guillement and R. Novikov, "A noise property analysis of single-photon emission computed tomography data", *Inverse Problems*, Vol. 20, pp. 175-198, 2004.

[11] M. Rabbani, "Bayesian filtering of Poisson noise using local statistics", *IEEE Trans. ASSP*, Vol. 36, pp. 933-936, 1988.

[12] S. Furuie and N. Mascarenhas, "Tomographic reconstruction of images with Poisson noise: projection estimation", *Automedica*, Vol. 15, pp. 133-140, 1992.

[13] C-M. Kao and X. Pan, "Fast implementation and quantitative evaluation of analytical methods with Wiener filters for image reconstruction in 3D SPECT", *IEEE Trans. Nucl. Science*, Vol. 46, pp. 1100-1109, 1999.

[14] H. Lu, J. Cheng, G. Han, L. Li, and Z. Liang, "A 3D distance-weighted Wiener filter for Poisson noise reduction in sinogram space for SPECT imaging", *SPIE Med. Imaging*, Vol. 4320, pp. 905-91, 2001.

[15] B.R. Hunt and O. Kübler, "K-L multi-spectral image restoration, part I: theory", *IEEE Trans. ASSP*, Vol. 32, pp. 592-600, 1984.

[16] M.N. Wernick, E.J. Infusino, and M. Milošević, "Fast spatio-temporal image reconstruction for dynamic PET", *IEEE Trans. Med. Imaging*, Vol. 18, pp. 185-195, 1999.

[17] M.V. Narayanan, M.A. King, M.N. Wernick, C.L. Byrne, E.J. Soares, and P.H. Pretorius, "Improved image quality and computation reduction in 4-D reconstruction of cardiac-gated SPECT images", *IEEE Trans Med. Imaging*, Vol. 19, pp. 423-433, 2000.

[18] H. Lu, D. Chen, G. Han, L. Li, and Z. Liang, "A combined transformation of ordering SPECT sinograms for signal extraction from measurements of Poisson noise", *SPIE Med. Imaging*, Vol. 4322, pp. 943-951, 2001.

[19] F.J. Anscombe, "The transformation of Poisson, binomial and negative-binomial data", *Biometrics*, Vol. 35, pp. 246-254, 1948.

[20] R. Kasturi, J.F. Walkup, and T.F. Krile, "Image restoration by transformation of signal-dependent noise to signal-independent noise", *Applied Optics*, Vol. 22, pp. 3537-3542, 1983.

[21] D.T. Kuan, A.A. Sawchuk, T.C. Strand, and P. Chavel, "Adaptive noise smoothing filter for image with signal-dependent noise", *IEEE Trans. PAMI*, Vol. 17, pp. 165-177, 1985.

[22] M. Pélégrini, H. Benali, G. El Fakhri, and et al, "Two-dimensional statistical model for regularized backprojection in SPECT", *Phys. Med. Biol.*, Vol. 43, pp. 421-434, 1998.

[23] H. Lu, I-T. Hsiao, X. Li and Z. Liang, "Spatial resolution uniformity of K-L transform on projection data along different directions for SPECT imaging", *J Nucl. Med.*, Vol. 42, pp.200P, 2001.

[24] J.A. Fessler and W.L. Rogers, "Spatial resolution properties of penalized-likelihood image reconstruction: space-invariant tomographs", *IEEE Trans. Image Processing*, vol. 5, pp. 1346-1358, 1996.

[25] P.J. La Rivière and X. Pan, "Nonparametric regression sinogram smoothing using a roughnes-penalized Poisson likelihood objective function", *IEEE Trans. Med. Imaging*, vol. 19, pp.773-786, 2000.

[26] J.W. Stayman and J.A. Fessler, "Compensation for nonuniform resolution using penalized-likelihood reconstruction in space-variant imaging systems", *IEEE Trans. Med. Imaging*, Vol. 23, pp. 269-284, 2004.